Complex variable boundary integral equations for perforated infinite planes

Helsing, Johan; Jonsson, Anders

Published in:
Engineering Analysis with Boundary Elements

DOI:
10.1016/S0955-7997(01)00006-6

2001

Complex variable boundary integral equations for perforated infinite planes

Johan Helsing and Anders Jonsson
Department of Solid Mechanics and NADA, Royal Institute of Technology,
SE-100 44 Stockholm, Sweden
Email: helsing@nada.kth.se, andersj@hallf.kth.se

December 5, 2000

Abstract

A fast and stable numerical algorithm is presented for the elastostatic problem of a linearly elastic plane with holes, loaded at infinity. The holes are free of stress. The algorithm is based on an integral equation which is intended as an alternative to the classic Sherman-Lauricella equation. The new scheme is argued to be both simpler and more reliable than schemes based on the Sherman-Lauricella equation. Improvements include simpler geometrical description, simpler relationships between mathematical and physical quantities, simpler extension to problems involving also inclusions and cracks, and more stable numerical convergence.

Key words: Linear elasticity, holes, integral equation of Fredholm type, fast multipole method, Sherman-Lauricella equation, effective elastic moduli, stress concentration factor, numerical methods, stable algorithms

1 Introduction

Perforated structures are commonly encountered in mechanical engineering and materials science. An important reason for perforation in mechanical design is to reduce weight. Other reasons are to facilitate ventilation and inspection. In materials science an objective is to reduce the occurrence of voids in order to improve material performance.

Perforation of a structure or a material often increases the local stress. Stress concentrations due to holes may result in reduced fatigue endurance or even in global structural collapse. Several engineering textbooks deal with stress concentration around holes (Neuber 1937; Savin 1961; Radaj and Schilberth 1977). In materials science, the over-all material properties are of interest. These properties are often described by a non-isotropic constitutive equation, which relates the average stress to the average strain by means of so called effective elastic moduli. The process of determining effective moduli is referred to as homogenization (Persson *et al.* 1993; Dvorak and Srinivas 1998). For a recent application to micromechanical modeling of cast iron, see Månson and Nilsson (2000).

In this paper we study perforated loaded planes numerically and compute local stresses and displacements. Also, we compute the effective elastic moduli using periodic boundary conditions. For reasons of stability and speed we prefer a method based on integral equations. There are several choices here, involving real variable notation with Green's functions for the stress and the displacement (Becker 1992) and complex variable notation with potential representation for the Airy stress function (Muskhelishvili 1953). The latter approach, which is our choice, may lead to the classic Sherman-Lauricella equation. See Greengard, Kropinski and Mayo (1996) for a comprehensive review.

The Sherman-Lauricella equation is a second kind Fredholm integral equation with compact operators. Despite its virtues, such as brevity of notation and that it gives stable numerical algorithms, we consider it awkward for two reasons. First, the Sherman-Lauricella equation requires the introduction of source terms at arbitrary points inside the holes and several arbitrary constants. This arbitrariness can substantially reduce numerical efficiency. It may be difficult to find the optimal choices of points and constants in practical applications. Second, the Sherman-Lauricella equation is based on representations of the Airy stress function which depend on the boundary conditions, and which are different from what has previously been used in crack- and bimaterial problems (Helsing and Peters 1999).

We will derive an integral equation for stress- and strain problems in a perforated plane that improves on the Sherman-Lauricella equation in four ways

- Unification of formulations: the same potential representation is used as in established equations for crack- and bimaterial problems.
- Simplified geometrical description: arbitrarily placed source points are not needed.
- Simplified post-processing: the layer density (unknown quantity) is related to physical quantities by simple expressions.
- Improved numerical efficiency: iterative algorithms based on the new equation require fewer iterations and exhibit slightly better stability.

The paper is organized as follows: Section 2 and 3 describe the elastostatic problem in words and in terms of partial differential equations. Section 4 introduces potential theory. The derivation of possible integral equations is outlined. Section 5 presents the classic Sherman-Lauricella equation. Section 6 presents our proposal for a new equation, which can be viewed as a special case of a bimaterial equation due to Sherman. The two equations are compared from a mathematical viewpoint in Section 7. Section 8 deals with the extraction of stress intensity factors and effective moduli from the solution. Section 9 contains details about numerical implementation. A numerical comparison between the two equations is undertaken in Section 10. The paper ends with Section 11 where we improve greatly on a recent numerical result (Ting, Chen, and Yang 1999) for two circular holes, and illustrate the extreme numerical stability of our scheme on a more challenging geometry.

2 The elastostatic problem

An infinite, linearly elastic plane is perforated with holes. The plane has two-dimensional elastic bulk and shear moduli κ and μ. There are N holes in the plane. The boundaries

of the holes are denoted Γ^j, $j = 1, \ldots, N$. The union of all boundaries is denoted Γ. The interior of the perforated plane is D_1 and the interior of all holes is D_2. Stress or strain is applied at infinity so that the average stress is $\bar{\sigma} = (\bar{\sigma}_{xx}, \bar{\sigma}_{yy}, \bar{\sigma}_{xy})$, or so that the average strain is $\bar{\epsilon} = (\bar{\epsilon}_{xx}, \bar{\epsilon}_{yy}, \bar{\epsilon}_{xy})$. The boundaries of the holes are free of stress.

We would like to compute displacement (u_x, u_y) and the stress- and strain fields in the material subject to three different imposed average stresses, namely $\bar{\sigma}_{\rm I} = (1, 0, 0)$, $\bar{\sigma}_{\rm II} = (0, 1, 0)$, and $\bar{\sigma}_{\rm III} = (0, 0, 1)$, or to three different imposed average strains, namely $\bar{\epsilon}_{\rm I} = (1, 0, 0)$, $\bar{\epsilon}_{\rm II} = (0, 1, 0)$, and $\bar{\epsilon}_{\rm III} = (0, 0, 1)$. We would also like to compute effective elastic moduli.

3 Partial differential equation formulation

We begin with a partial differential equation formulation for our problem. We present it as a mathematically equivalent alternative to the integral equations used later on.

Insertion of the definition of the linear strain tensor and the constitutive equation relating the strains to the stresses into the equation of static equilibrium yields a coupled system of second order elliptic equations for the displacement field (Navier's equation)

$$\mu u_{i,jj} + \kappa u_{j,ji} = 0\,, \qquad i = 1, 2\,. \tag{1}$$

The boundary condition on Γ is

$$\left(\mu(u_{i,j} + u_{j,i}) + (\kappa - \mu)u_{k,k}\delta_{ij}\right) n_j = 0\,, \qquad i = 1, 2\,, \tag{2}$$

where (n_x, n_y) is the normal unit vector on Γ. The plane is loaded by stress or strain which is applied at infinity so that their area averages assume prescribed values

$$\bar{\sigma}_{ij} \equiv < \mu(u_{i,j} + u_{j,i}) + (\kappa - \mu)u_{k,k}\delta_{ij} > = \sigma_{ij}^{\rm presc}\,, \qquad i, j = 1, 2\,, \tag{3}$$

or

$$\bar{\epsilon}_{ij} \equiv < (u_{i,j} + u_{j,i})/2 > = \epsilon_{ij}^{\rm presc}\,, \qquad i, j = 1, 2\,. \tag{4}$$

The components of $\sigma_{ij}^{\rm presc}$ or $\epsilon_{ij}^{\rm presc}$ are given by the components of the applied load $\bar{\sigma}_{\rm I}$, $\bar{\sigma}_{\rm II}$, $\bar{\sigma}_{\rm III}$, $\bar{\epsilon}_{\rm I}$, $\bar{\epsilon}_{\rm II}$, or $\bar{\epsilon}_{\rm III}$.

4 Potential representation

It is natural to introduce the Airy stress function U, which solves the equation of static equilibrium by definition. From the assumption that certain sequences of partial derivative operators commute when acting on u_x and on u_y (compatibility equations), it follows that U is biharmonic (except for at Γ). Airy's stress function can be represented as

$$U = \Re{\rm e}\left\{\bar{z}\phi + \chi\right\}\,, \tag{5}$$

where the potentials ϕ and χ are single valued analytic functions of the complex variable $z = x + iy$. For a thorough discussion of the complex variable approach to elasticity problems, see Muskhelishvili (1953), Sokholnikoff (1956), Mikhlin (1957), or Parton and

Perlin (1982). For our purposes it is sufficient to observe a few relations that link the complex potentials to quantities of physical interest. The displacement (u_x, u_y) in the material satisfies

$$u_x + iu_y = \left(\frac{1}{2\mu} + \frac{1}{\kappa}\right)\phi - \frac{1}{2\mu}\left(z\overline{\phi'} + \overline{\psi}\right), \tag{6}$$

where $\psi = \chi'$. The integral of the traction (t_x, t_y) along a curve $\gamma(s)$ with normal (n_x, n_y) can be obtained from

$$\int_{s_0}^{s} (t_x + it_y)\mathrm{d}s = -\Big|_{s_0}^{s} i\left(\phi + z\overline{\phi'} + \overline{\psi}\right), \tag{7}$$

where s denotes arclength along $\gamma(s)$.

The components of the stress tensor can be computed via

$$\sigma_{xx} + \sigma_{yy} = 4\Re\mathrm{e}\{\phi'\}, \tag{8}$$

$$\sigma_{yy} - \sigma_{xx} + 2i\sigma_{xy} = 2(\bar{z}\phi'' + \psi'). \tag{9}$$

A standard starting point for elastostatic problems is to represent the potentials ϕ and ψ in the form of Cauchy-type integrals

$$\phi(z) = \frac{1}{2\pi i}\int_\Gamma \frac{\omega(\tau)\mathrm{d}\tau}{(\tau - z)} + \frac{\alpha z}{2}, \qquad z \in D_1, \tag{10}$$

and

$$\psi(z) = \frac{1}{2\pi i}\int_\Gamma \frac{\rho(\tau)\mathrm{d}\tau}{(\tau - z)} + \beta z, \qquad z \in D_1, \tag{11}$$

where ω and ρ are unknown layer densities and α and β are forcing terms. Values of ϕ and ψ on Γ are defined as limits of ϕ and ψ in D_1 as Γ is approached. Since the equations of elasticity now are satisfied everywhere, it remains only to solve the problem which consists of enforcing the boundary condition of zero traction along Γ.

The constants α and β in (10) and (11) represent the forcing terms at infinity. When average stress is imposed, the constants take the values $\alpha = 1/2$ and $\beta = -1/2$ for $\bar{\sigma}_{\mathrm{I}}$, the values $\alpha = 1/2$ and $\beta = 1/2$ for $\bar{\sigma}_{\mathrm{II}}$, and the values $\alpha = 0$ and $\beta = i$ for $\bar{\sigma}_{\mathrm{III}}$. When average strain is imposed, the constants take the values $\alpha = \kappa$ and $\beta = -\mu$ for $\bar{\epsilon}_{\mathrm{I}}$, the values $\alpha = \kappa$ and $\beta = \mu$ for $\bar{\epsilon}_{\mathrm{II}}$, and the values $\alpha = 0$ and $\beta = 2i\mu$ for $\bar{\epsilon}_{\mathrm{III}}$. Thus, α can always be assumed to be real, while β is either a real or an imaginary number.

5 The Sherman-Lauricella integral equation

The classical way of solving the elastostatic equation is by expressing ρ of (11) in terms of ω of (10) in a way which makes ψ assume the form

$$\psi(z) = \frac{1}{2\pi i}\int_\Gamma \frac{\omega(\tau)\mathrm{d}\bar{\tau}}{(\tau - z)} + \frac{1}{2\pi i}\int_\Gamma \frac{\overline{\omega(\tau)}\mathrm{d}\tau}{(\tau - z)} - \frac{1}{2\pi i}\int_\Gamma \frac{\bar{\tau}\omega(\tau)\mathrm{d}\tau}{(\tau - z)^2} + \sum_{j=1}^{N}\frac{b_j}{z - z_j} + \beta z, \tag{12}$$

where z_j is an arbitrary point inside the hole bounded by Γ^j and the source terms $b_j/(z-z_j)$ are needed to ensure that the resulting integral equation is solvable. The real constants b_j are related to ω by

$$b_j = k\Im\mathrm{m}\left\{\int_{\Gamma^j}\omega(z)\mathrm{d}\bar{z}\right\}, \tag{13}$$

where k is an arbitrary real non-zero constant, usually chosen as $k=-2$. The representations (10) for ϕ and (12) for ψ were first derived by Lauricella (1909) and further developed by Sherman (1940).

The choice of the representation (12) for ψ can be motivated by the fact that it leads to an equation of Fredholm's second kind. The requirement of zero traction on Γ^j gives, via (7), (10) and (12), the Sherman-Lauricella integral equation

$$(I-M_{\mathrm{SL}})\,\omega(z) - \sum_{j=1}^{N}\frac{b_j}{\bar{z}-\bar{z}_j} - C_j = \alpha z + \bar{\beta}\bar{z}\,, \qquad z\in\Gamma^j\,, \tag{14}$$

where M_{SL} is a compact integral operator given by

$$M_{\mathrm{SL}}\omega(\tau) = \frac{1}{2\pi i}\left[\int_\Gamma\frac{\omega(\tau)\mathrm{d}\tau}{\tau-z} - \int_\Gamma\frac{\omega(\tau)\mathrm{d}\bar{\tau}}{\bar{\tau}-\bar{z}} - \int_\Gamma\frac{\overline{\omega(\tau)}\mathrm{d}\tau}{\bar{\tau}-\bar{z}} + \int_\Gamma\frac{(\tau-z)\overline{\omega(\tau)}\mathrm{d}\bar{\tau}}{(\bar{\tau}-\bar{z})^2}\right], \qquad z\in\Gamma\,, \tag{15}$$

and C_j are complex constants, related to ω via

$$C_j = k_j\int_{\Gamma^j}\omega(\tau(s))\mathrm{d}s\,, \tag{16}$$

where k_j are arbitrary non-zero complex constants, usually chosen as $k_j=1$.

The displacement of (6) at Γ^j is given by

$$u_x+iu_y = \left(\frac{1}{\kappa}+\frac{1}{\mu}\right)\left(\frac{1}{2\pi i}\int_\Gamma\frac{\omega(\tau)\mathrm{d}\tau}{(\tau-z)} - \frac{\omega(z)}{2} + \frac{\alpha z}{2}\right) - \frac{C_j}{2\mu}\,, \qquad z\in\Gamma^j\,. \tag{17}$$

Proofs of solvability and uniqueness of (14) can be found in Muskhelishvili (1953), Mikhlin (1957), and Parton and Perlin (1982). The particular choices of z_j in (12), k in (13), and k_j in (16) do not change the value of the potentials ϕ and ψ in the interior of the perforated plane. They do, however, change the value of ω, and they will influence the performance of iterative numerical schemes based on equation (14). The standard choices $k=-2$ and $k_j=1$ seem to be reasonably efficient from a numerical viewpoint.

Remark 5.1 Sherman has three different choices for ψ depending on the boundary conditions, leading to three different integral equations. If the holes are free from stress and the loads are applied only at infinity, the equation for prescribed stress (14) can handle both the case of prescribed average stress and the case of prescribed average strain.

Remark 5.2 Representations for the potentials ϕ and ψ do not necessarily have to be on the form of Cauchy-type integrals and lead to integral equations. Another possibility is to represent the potentials in terms of Laurent series and to derive algebraic equations for their coefficients. See Vigdergauz (1999) for a recent example.

6 The Sherman bimaterial equation

An interesting option, introduced by Sherman (1959) for bimaterials, is to extend the validity of ϕ of (10) and ψ of (11) into the holes D_2, and to choose the unknown layer densities ω of (10) and ρ of (11) in such a way that the expression for the integral of traction (7) is continuous over Γ. This requirement allows us to express ρ in terms of ω, and ψ assumes the form

$$\psi(z) = \frac{1}{2\pi i}\int_\Gamma \frac{\omega(\tau)\mathrm{d}\bar{\tau}}{(\tau - z)} - \frac{1}{2\pi i}\int_\Gamma \frac{\overline{\omega(\tau)}\mathrm{d}\tau}{(\tau - z)} - \frac{1}{2\pi i}\int_\Gamma \frac{\bar{\tau}\omega(\tau)\mathrm{d}\tau}{(\tau - z)^2} + \beta z\,. \tag{18}$$

The requirement of zero traction along Γ leads to the integral equation for ω

$$(M_1 - M_2)\omega(z) = -\alpha z - \bar{\beta}\bar{z} - c_j\,, \quad z \in \Gamma^j\,, \tag{19}$$

where c_j are complex constants of consistency, and M_1 and M_2 are integral operators given by

$$M_1\omega(z) = \frac{1}{\pi i}\int_\Gamma \frac{\omega(\tau)\mathrm{d}\tau}{(\tau - z)}\,, \qquad z \in \Gamma\,, \tag{20}$$

and

$$M_2\omega(\tau) = \frac{1}{2\pi i}\left[\int_\Gamma \frac{\omega(\tau)\mathrm{d}\tau}{(\tau - z)} - \int_\Gamma \frac{\omega(\tau)\mathrm{d}\bar{\tau}}{(\bar{\tau} - \bar{z})} + \int_\Gamma \frac{\overline{\omega(\tau)}\mathrm{d}\tau}{(\bar{\tau} - \bar{z})} - \int_\Gamma \frac{(\tau - z)\overline{\omega(\tau)}\mathrm{d}\bar{\tau}}{(\bar{\tau} - \bar{z})^2}\right]\,, \qquad z \in \Gamma\,. \tag{21}$$

Two properties of M_2 are easy to prove

$$M_2 c = c\,, \tag{22}$$

$$M_2 iz = iz\,, \tag{23}$$

where c is a constant. Since constants and iz are eigenfunctions with eigenvalue unity also to the operator M_1, equations (22) and (23) imply that (19) is not uniquely solvable, but that is has two simple null-functions. We therefore add the uniqueness condition

$$(I + M_1)\omega(z) = -\alpha z - (1 - d_j)c_j\,, \quad z \in \Gamma^j\,. \tag{24}$$

where d_j is an arbitrary constant. Linear combinations of (19) and (24) gives that ω satisfies

$$\left(I + d_j M_1 + (1 - d_j)M_2\right)\omega(z) = -d_j\alpha z + (1 - d_j)\bar{\beta}\bar{z}\,, \qquad z \in \Gamma^j\,, \tag{25}$$

which is our proposal for a new equation. Note that the constants of consistency, c_j, of (19) and (24) do not appear in (25). That (25) is uniquely solvable follows from Fredholm's alternative and the discussion in paragraph 4 of Sherman (1959). In fact, equation (25) can be derived directly from the Sherman bimaterial equation (1959) by letting the bulk and shear moduli κ_j and μ_j of inclusion j in the bimaterial approach zero in such a way that their ratio is constant. The Sherman bimaterial integral equation then assumes the form (25) with $d_j = \mu_j/(\mu_j + \kappa_j)$.

The displacement of (6) at the boundary Γ^j is particularly easy to evaluate in our setting,

$$u_x + iu_y = -\omega_j \left(\frac{1}{\kappa} + \frac{1}{\mu} \right) + \frac{c_j}{2} \left(\frac{(d_j - 1)}{\kappa} + \frac{d_j}{\mu} \right) . \tag{26}$$

The solution ω to (25) is independent of d_j (up to a constant on each Γ^j). In the limits $d_j \to 0$ and $d_j \to 1$, however, equation (25) becomes singular. For certain values of d_j the conditioning of (25) is optimal. An interesting choice is $d_j = \mu/(\mu + \kappa)$. This choice makes the displacement of (26) directly proportional to ω. More generally, we have found that $d_j > 0.5$ can cause an unnecessary large number of iterations in the process of solving (25) iteratively. A value in the range $0.10 < d_j < 0.35$ seems to be a good general choice.

Remark 6.1 The equation (25) contains the Cauchy singular operator M_1 which is non-compact on a single, closed contour. This is not a problem from a computational viewpoint. The operator M_1 resembles the identity. Further, it is possible to transform equation (25) into a Fredholm second kind equation with compact operators by application of the operator $(I - d_j M_1^j)/(1 - d_j^2)$, where M_1^j denotes the restriction of M_1 to Γ^j. The part of M_1 which describes interaction between different contours is always compact.

7 Relationships between equations

The Sherman-Lauricella equation (14) and equation (25) look different. The Sherman-Lauricella equation contains the choice of N arbitrarily placed points and $N + 1$ arbitrarily chosen constants, while equation (25) contains only N arbitrarily chosen constants. The Sherman-Lauricella equation only contain compact operators, while equation (25) contains the Cauchy singular operator M_1. The expression for the displacement (17) in the Sherman-Lauricella framework is more complicated to evaluate than our expression (26).

A relation between the layer densities of the two equations can be derived by equating (17) and (26). The choice $d_j = \mu/(\mu + \kappa)$ gives the simplest form of this relation

$$\omega(z) = \frac{1}{2} \left(I - M_1 \right) \omega_{SL}(z) - \frac{\alpha z}{2} - \frac{C_j}{2(1 + \mu/\kappa)}, \qquad z \in \Gamma^j, \tag{27}$$

where ω_{SL} denotes the layer density of the Sherman-Lauricella equation and ω denotes the layer density of equation (25). Equation (27) can not be inverted, that is, give ω_{SL} as a function of ω. The density ω_{SL} has, in general, a more complicated structure than the density ω. As a consequence, we expect iterative algorithms based on the Sherman-Lauricella equation to converge slower than iterative algorithms based on equation (25). See Section 10 for examples where such a difference in convergence rate is observed.

8 Effective moduli and stress tensor on the boundary

Effective elastic moduli are particularly simple to define and compute in the setting of a doubly periodic material with a square unit cell of unit area. The effective compliance

moduli of a material can be defined through the following relations between average stress and average strain

$$\begin{pmatrix} \bar{\epsilon}_{xx} \\ \bar{\epsilon}_{yy} \\ \sqrt{2}\bar{\epsilon}_{xy} \end{pmatrix} = \begin{pmatrix} s_{*1} & s_{*2} & s_{*3} \\ s_{*2} & s_{*4} & s_{*5} \\ s_{*3} & s_{*5} & s_{*6} \end{pmatrix} \begin{pmatrix} \bar{\sigma}_{xx} \\ \bar{\sigma}_{yy} \\ \sqrt{2}\bar{\sigma}_{xy} \end{pmatrix}. \tag{28}$$

The components of the effective compliance tensor S are s_{*k}, $k = 1, \ldots, 6$.

In order to compute the effective compliance tensor S, equation (25) is solved three times for the imposed average stresses $\bar{\sigma}_{\mathrm{I}}$, $\bar{\sigma}_{\mathrm{II}}$ and $\bar{\sigma}_{\mathrm{III}}$. The corresponding solutions are denoted as ω_{I}, ω_{II} and ω_{III}. Let now

$$a_{\mathrm{K}} = \frac{1}{2}\left(\frac{1}{\kappa} + \frac{1}{\mu}\right) \int_{\Gamma_u} \omega_{\mathrm{K}}(z)\mathrm{d}z\,, \qquad \mathrm{K} = \mathrm{I}, \mathrm{II}, \mathrm{III}\,, \tag{29}$$

and

$$b_{\mathrm{K}} = \frac{1}{2}\left(\frac{1}{\kappa} + \frac{1}{\mu}\right) \int_{\Gamma_u} \omega_{\mathrm{K}}(z)\mathrm{d}\bar{z}\,, \qquad \mathrm{K} = \mathrm{I}, \mathrm{II}, \mathrm{III}\,. \tag{30}$$

With this notation, the effective compliance tensor of equation (28) can be computed as

$$S = \frac{1}{4\kappa\mu} \begin{pmatrix} \kappa+\mu & \mu-\kappa & 0 \\ \mu-\kappa & \kappa+\mu & 0 \\ 0 & 0 & 2\kappa \end{pmatrix} + \Im\mathrm{m} \begin{pmatrix} b_{\mathrm{I}} - a_{\mathrm{I}} & b_{\mathrm{II}} - a_{\mathrm{II}} & \frac{1}{\sqrt{2}}(b_{\mathrm{III}} - a_{\mathrm{III}}) \\ a_{\mathrm{I}} + b_{\mathrm{I}} & a_{\mathrm{II}} + b_{\mathrm{II}} & \frac{1}{\sqrt{2}}(a_{\mathrm{III}} + b_{\mathrm{III}}) \\ i\sqrt{2}a_{\mathrm{I}} & i\sqrt{2}a_{\mathrm{II}} & ia_{\mathrm{III}} \end{pmatrix}. \tag{31}$$

The inverse of the effective compliance tensor is the effective stiffness tensor C whose components c_{*k}, $k = 1, \ldots, 6$, are defined through the following relation

$$\begin{pmatrix} \bar{\sigma}_{xx} \\ \bar{\sigma}_{yy} \\ \sqrt{2}\bar{\sigma}_{xy} \end{pmatrix} = \begin{pmatrix} c_{*1} & c_{*2} & c_{*3} \\ c_{*2} & c_{*4} & c_{*5} \\ c_{*3} & c_{*5} & c_{*6} \end{pmatrix} \begin{pmatrix} \bar{\epsilon}_{xx} \\ \bar{\epsilon}_{yy} \\ \sqrt{2}\bar{\epsilon}_{xy} \end{pmatrix}. \tag{32}$$

In order to compute the effective stiffness tensor, equation (25) is solved three times for the imposed average strains $\bar{\epsilon}_{\mathrm{I}}$, $\bar{\epsilon}_{\mathrm{II}}$ and $\bar{\epsilon}_{\mathrm{III}}$. The corresponding solutions are denoted as ω_{I}, ω_{II} and ω_{III}. Let now

$$a_{\mathrm{K}} = \left(1 + \frac{\mu}{\kappa}\right) \int_{\Gamma_u} \omega_{\mathrm{K}}(z)\mathrm{d}z\,, \qquad \mathrm{K} = \mathrm{I}, \mathrm{II}, \mathrm{III}\,, \tag{33}$$

and

$$b_{\mathrm{K}} = \left(1 + \frac{\kappa}{\mu}\right) \int_{\Gamma_u} \omega_{\mathrm{K}}(z)\mathrm{d}\bar{z}\,, \qquad \mathrm{K} = \mathrm{I}, \mathrm{II}, \mathrm{III}\,. \tag{34}$$

The effective stiffness tensor of equation (32) can then be computed as

$$C = \begin{pmatrix} \kappa+\mu & \kappa-\mu & 0 \\ \kappa-\mu & \kappa+\mu & 0 \\ 0 & 0 & 2\mu \end{pmatrix} - \Im\mathrm{m} \begin{pmatrix} b_{\mathrm{I}} - a_{\mathrm{I}} & b_{\mathrm{II}} - a_{\mathrm{II}} & \frac{1}{\sqrt{2}}(b_{\mathrm{III}} - a_{\mathrm{III}}) \\ a_{\mathrm{I}} + b_{\mathrm{I}} & a_{\mathrm{II}} + b_{\mathrm{II}} & \frac{1}{\sqrt{2}}(a_{\mathrm{III}} + b_{\mathrm{III}}) \\ i\sqrt{2}a_{\mathrm{I}} & i\sqrt{2}a_{\mathrm{II}} & ia_{\mathrm{III}} \end{pmatrix}. \tag{35}$$

The components of the stress tensor σ_{ij} in (8) and (9) take the following form on the boundary Γ in terms of our density ω

$$\sigma_{xx} + \sigma_{yy} = -4\Re\mathrm{e}\left\{\frac{\mathrm{d}\omega}{\mathrm{d}z}\right\}, \tag{36}$$

$$\sigma_{yy} - \sigma_{xx} + 2i\sigma_{xy} = -4\frac{\bar{n}}{n}\Re\mathrm{e}\left\{\frac{\mathrm{d}\omega}{\mathrm{d}z}\right\}. \tag{37}$$

The traction (t_x, t_y) on the boundary Γ can be obtained from

$$t_x + it_y = -4in\Re\mathrm{e}\left\{\frac{\mathrm{d}\omega}{\mathrm{d}z}\right\}. \tag{38}$$

Other quantities, useful when dealing with the stress fields in the vicinity of the holes, are the normalized tangential stress σ_{tn} and the stress concentration factor K_t. The normalized tangential stress is defined as the ratio of the tangential stress on the boundary of a hole to the trace of the applied stress tensor

$$\sigma_{\mathrm{tn}} = \frac{4\Re\mathrm{e}\{\frac{\mathrm{d}\omega}{\mathrm{d}z}\}}{\mathrm{Tr}\{\bar{\sigma}_{\mathrm{appl}}\}}. \tag{39}$$

The stress concentration factor is defined as the maximum absolute value of the normalized tangential stress

$$K_t = \max_{z\in\Gamma} |\sigma_{\mathrm{tn}}|. \tag{40}$$

9 Nyström algorithm and singular integrals

In the next two sections we solve equations (14) and (25) for a variety of geometries and loads. In most examples we shall use a "matrix-free" Nyström algorithm based on composite 16-point Gaussian quadrature, the GMRES iterative solver (Saad and Schultz 1986), the fast multipole method (Rokhlin 1985; Greengard and Rokhlin 1987; Carrier *et al.* 1988), and a special scheme for the evaluation of layer potentials close to their sources (Helsing 1996). Compensated summation (Kahan 1965; Higham 1996) is used for the computation of inner products in the GMRES solver and for the evaluation of the integrals appearing in the formulas for effective moduli. We refer to Greengard and Helsing (1998) for further implementational details. Here we will discuss a particular refinement implemented in the present code. It concerns the regularization of the singular integral appearing in (20).

It is easy to verify the following: Let $f(z)$ be a smooth function on Γ and let a and b be two points on Γ. Then

$$\frac{1}{\pi i}\int_a^b \frac{f(\tau)\mathrm{d}\tau}{(\tau - z)} =$$

$$\frac{1}{\pi}\int_a^b f(\tau)\Re\mathrm{e}\left\{\frac{\mathrm{d}\tau}{i(\tau - z)}\right\} + \frac{i}{\pi}\int_a^b (f(\tau) - f(z))\Im\mathrm{m}\left\{\frac{\mathrm{d}\tau}{i(\tau - z)}\right\} + \frac{f(z)}{\pi i}\Re\mathrm{e}\left\{\ln\left[\frac{a - z}{b - z}\right]\right\}. \tag{41}$$

The first integral on the right hand side of (41) has a smooth kernel. The second integral has a smooth integrand. The third term is easy to evaluate.

Now, let z be a target point on a quadrature panel Γ_0 on Γ. Further, let $\Gamma_{0-\mathrm{left}}$ and $\Gamma_{0-\mathrm{right}}$ be quadrature panels adjacent to Γ_0. Let $\Gamma_{0-\mathrm{other}}$ be the union of all other quadrature panels. For the evaluation of

$$\frac{1}{\pi i}\int_\Gamma \frac{f(\tau)\mathrm{d}\tau}{(\tau - z)}, \qquad z \in \Gamma_0,$$

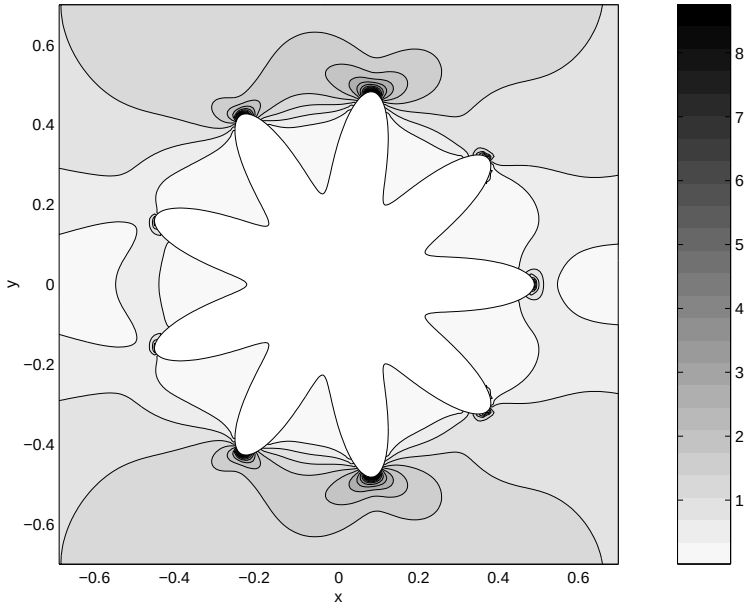

Figure 1: The von Mises effective stress distribution for an infinite plate with a starfish-shaped hole under imposed stress $\overline{\sigma}_I$. The stress concentration factor of (40) for the hole is $K_t = 9.233388765$.

we distinguish between two cases. For the part of the integral that contains contributions from $\Gamma_{0-\text{other}}$, we evaluate the integral as it stands. For the part of the integral that contain contributions from $\Gamma_{0-\text{left}}$, Γ_0, and $\Gamma_{0-\text{right}}$, we use the right hand side of (41), with a being the starting-point on $\Gamma_{0-\text{left}}$ and with b being the end-point on $\Gamma_{0-\text{right}}$.

10 Numerical comparison between equations

Some differences between the Sherman-Lauricella equation (14) and equation (25) have been pointed out in Remark 6.1 and in Section 7. In this section we undertake a detailed comparison between algorithms based on the two equations, to see what consequences these differences have for numerical efficiency. The experiments presented indicate that equation (25) leads to a better algorithm.

For setups with analytical solutions, such as loaded plates with a single hole in the shape of a circle or an ellipse, it is hard to say which equation leads to the best algorithm. Algorithms based on the two equations both require only a few GMRES iterations for full convergence. A non-trivial example is needed. We therefore consider a plate with one single hole in the shape of a nine-armed starfish parameterized by

$$z(t) = 0.36(1 + 0.36\cos 9t)e^{it}\,, \qquad -\pi \leq t < \pi\,, \tag{42}$$

under the imposed average stress $\overline{\sigma}_I$, see Figure 1. This shape might seem spectacular at first glance, but similar shapes are used in, for example, spline couplings (a machine element). Figure 1 also shows contours of the distribution of the von Mises effective stress

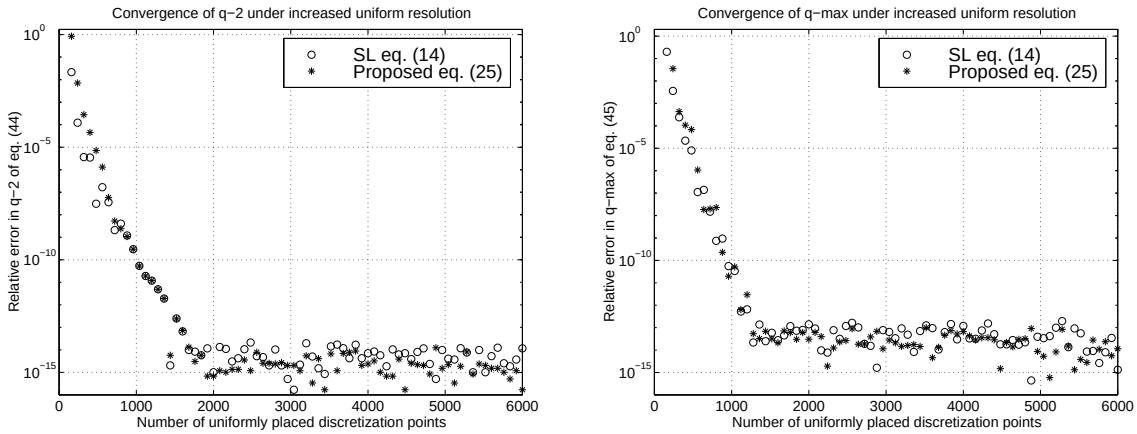

Figure 2: Convergence of the reference quantities q_2 of (44) and $q_{\max}$ of (45) for algorithms based on equations (14) and (25). Correct values, computed in quadruple precision arithmetic, are $q_2 = 0.6540490820646557$ and $q_{\max} = 0.3762294219389333$. The relative error for values of q_2 and $q_{\max}$ that coincide with the correct value is displayed as $1.11 \cdot 10^{-16}$.

σ_{eM}. The von Mises effective stress is used to predict the occurrence of plastic deformation in a multiaxial state of stress. For plane stress, it is defined by

$$\sigma_{eM} = \sqrt{\sigma_{xx}^2 + \sigma_{yy}^2 - \sigma_{xx}\sigma_{yy} + 3\sigma_{xy}^2}\,. \tag{43}$$

When comparing the performance of the algorithms below, we need reference quantities to measure accuracy against. We have decided to use the L^2 norm of a normalized boundary displacement

$$q_2 = \frac{\mu\kappa}{\mu+\kappa}\left(\int_\Gamma \left(u_x^2(z) + u_y^2(z)\right) \mathrm{d}s\right)^{\frac{1}{2}}\,, \tag{44}$$

and also the maximum value of a normalized boundary displacement

$$q_{\max} = \frac{\mu\kappa}{\mu+\kappa} \max_{z\in\Gamma} \left(u_x^2(z) + u_y^2(z)\right)^{\frac{1}{2}}\,, \tag{45}$$

as such reference quantities. One could, of course, also use some Sobolev norm of the boundary displacement, or measure the convergence of the displacement field itself. Using such procedures, it would be harder to detect differences between the algorithms. Numerical differentiation and interpolation between meshes introduce additional error.

The quantity q_2 is particularly simple to compute and tells us, perhaps, most about the quality of the solution. The quantity q_2 can be extracted from the solutions ω_{SL} to (14) and ω to (25) via (17) and (26) and with the use of integration at the nodes where ω_{SL} and ω have support. The quantity $q_{\max}$ requires more post-processing. This is so since the maximum displacement does not necessarily occur at a quadrature node. We extract $q_{\max}$ by 15th order polynomial interpolation followed by golden section search. The bulk and shear moduli are chosen so that $\mu/(\mu+\kappa) = 0.23$.

An algorithm based on equation (25) requires 1760 discretization points for a relative error in q_2 smaller than 10^{-14} and for a relative error in $q_{\max}$ smaller than 10^{-13}, see Figure 2.

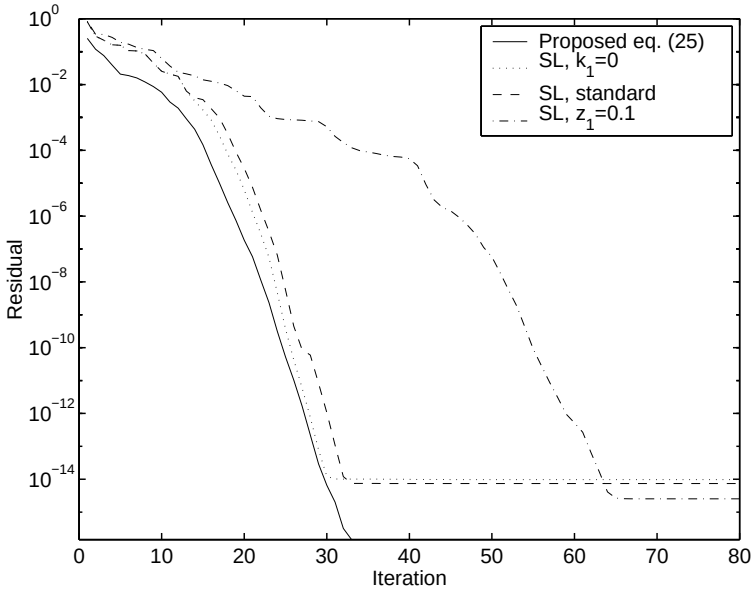

Figure 3: The iteration history from GMRES for the different integral formulations. 2080 discretization points were used.

Solving the system of linear equations at full resolution, that is with 2080 discretization points, requires 30 GMRES iterations with the choice $d_1 = 0.23$. The particular choice of $d_1 = 0.23$ seems in this case quite good. Other values of d_1 also work well for this geometry and load. Numerical experiments show that values in the range $0.004 < d_1 < 0.76$ yield a solution with a relative error in q_2 smaller than 10^{-14}. For values of d_1 below 0.1 and above 0.3, however, the number of GMRES iterations increases.

An algorithm based on the Sherman-Lauricella integral equation (14), with standard choices of the constants k of (13) and k_1 of (16) and the arbitrary point z_1 placed at the origin, also requires 1760 discretization points to reach a relative error in q_2 of about 10^{-14} and a relative error in $q_{\max}$ of about 10^{-13}. The number of GMRES iterations required with 2080 points is 33. This performance, however, can be slightly improved. In fact, in this example, it is possible to choose $k_1 = 0$. This choice reduces the number of GMRES iterations needed to 30 without affecting the accuracy. Most other choices of k_1 within reasonable limits ($|k_1| < 100$) give 33 GMRES iterations without affecting the quality of the solution. Note that the choice $k_1 = 0$ is possible here because the geometry and load are such that the integral in (16) vanishes. Note also that $k_1 = 0$ renders the integral equation (14) singular with rank deficiency two. It allows for null-solutions being complex constants. The system of linear equations is, obviously, unsolvable with a direct method. In our case, a correct solution is obtained since an iterative solver is used. The right hand side of (14) lies in the range of the integral operator of the modified equation. The choices for the premultiplying factor k are more restricted. Only k in the interval $1 \leq |k| \leq 4$ give an accurate solution.

The starfish in Figure 1 is symmetric with respect to the origin. A natural choice for the arbitrary point is therefore $z_1 = 0$. In more complicated geometries there might not be

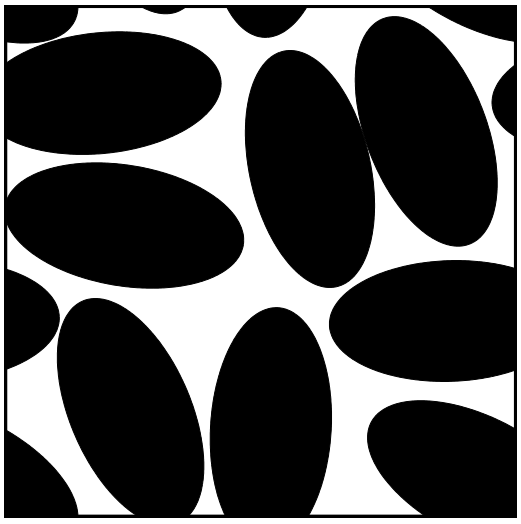

Figure 4: A unit cell consisting of a plate with eight elliptical holes (black) of aspect ratio 2:1 at ellipse area fraction 0.7.

such a simple and natural choice. The numerical performance of the Sherman-Lauricella equation is sensitive to the choice of z_1. If we set $z_1 = 0.1$, which still is far away from the boundary of the starfish contour, the number of GMRES iterations doubles, see Figure 3, and the relative errors in q_2 and $q_{\max}$ increase.

Further differences in the numerical performance of the two algorithms, and for the choices $d_1 = 0.23$, $k = -2$, $k_1 = 1$, $z_1 = 0$, can be pointed out. First, the algorithm based on equation (25) requires fewer iterations than the algorithm based on the Sherman-Lauricella equation for reaching a given residual in the GMRES solver. It is also possible to reach a lower residual with equation (25). This is illustrated in Figure 3. Second, the convergence of the solution with the number of discretization points is initially somewhat slower for the algorithm based on equation (25) than that for the algorithm based on the Sherman-Lauricella equation. Third, the algorithm based on equation (25) seems to be more stable in the sense that when the number of discretization points is increased beyond 1760, the reference quantity q_2 converges more stably when computed from ω of (25) than from ω_{SL} of the Sherman-Lauricella equation. The effect on $q_{\max}$ is similar, but less pronounced. This is illustrated in Figure 2.

We conclude that an algorithm based on equation (25) is generally slightly more efficient than an algorithm based on the Sherman-Lauricella equation (14). The chief reason for this is that we have omitted the need for the arbitrary point z_1. A poor choice of z_1 can greatly deteriorate the performance of algorithms based on the Sherman-Lauricella equation.

11 Numerical examples

In this section we shall present more examples of numerical solutions to equation (25). We shall first establish agreement with results of previous investigators. Then we shall demonstrate the extreme stability of our algorithm.

Table 1: Center coordinates x_{cent}, y_{cent}, and rotations α for the eight ellipses depicted in Figure 4.

ellipse no.	x_{cent}	y_{cent}	α
1	0.096558008044553	0.180606440983544	1.793069456776903
2	-0.312317331860957	0.328928705317157	0.103527236861962
3	0.020093822024223	-0.326279205482295	-1.631099491555291
4	0.426052439830122	-0.422860540089244	-0.473183135086323
5	0.323978421616729	0.254064864498771	-1.204877840652208
6	-0.266711719264471	0.070034693393812	-0.162392923788297
7	0.370486724007364	-0.116660224915378	0.034300608334877
8	-0.254250775518318	-0.294308693171502	1.979465648427812

Table 2: Converged values of effective elastic moduli for the plate with elliptical holes in Figure 4. The elastic moduli of the plate are $\mu = 1$ and $\kappa = 3\frac{1}{3}$. Digits within parentheses are uncertain.

c_{*1}	0.1671838860540(3)
c_{*2}	0.1159038641252(6)
c_{*3}	-0.0334596680291(2)
c_{*4}	0.2145913741192(2)
c_{*5}	-0.0541949785279(8)
c_{*6}	0.0500907100757(7)

11.1 Two circular holes in an infinite plate

We start out with a very simple configuration: an infinite plate with two circular holes of radius unity, aligned with the x-axis, and separated with a distance of 0.2. The stress $\bar{\sigma}_{\text{II}}$ is applied. This setup has been studied by Haddon (1967) and more recently by Ting, Chen, and Yang (1999). Quantities studied by these authors include the normalized tangential stress σ_{tn} of (39) and the stress concentration factor K_t of (40). The value of the stress concentration factor is reported as $K_t = 6.106$ by Haddon (1967) and as $K_t = 6.107$ by Ting, Chen, and Yang (1999). With 80 uniformly placed discretization points on each of the two hole boundaries we reproduce Haddon's estimate $K_t = 6.106$. A more accurate estimate is $K_t = 6.106040764542$, which we get with 400 uniformly placed discretization points on each hole boundary.

11.2 Eight elliptical holes in a doubly periodic arrangement

Figure 4 shows a unit cell of a plate with eight equi-sized elliptical holes. The unit cell is periodically repeated as to tile the entire plane. The aspect ratio of the axes of the ellipses is 2:1. The area fraction of the elliptical holes is 0.7. The elastic moduli of the plate are

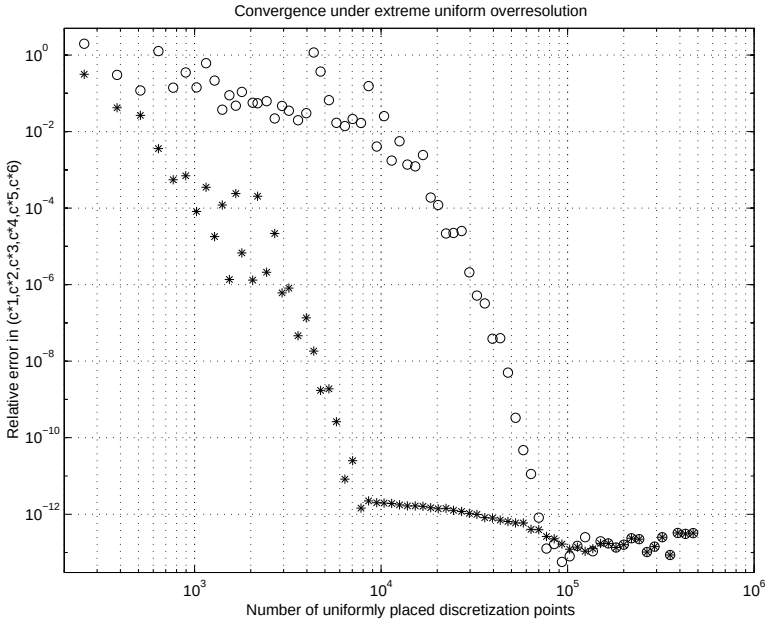

Figure 5: Convergence of the Euclidean norm of a vector with effective elastic moduli, defined in (32), for the geometry in Figure 4, under uniform overresolution. Stars refer to calculations where a special scheme for the evaluation of layer potentials close to their sources is used when needed. Open circles refer to calculations without this special scheme. The values in Table 2 are used as reference.

$\mu = 1$ and $\kappa = 3\frac{1}{3}$. Each ellipse has the parameterization

$$z(t) = z_{\text{cent}} + \sqrt{\frac{0.7}{16\pi}} e^{i\alpha}(2\cos t + i \sin t), \qquad -\pi \leq t < \pi. \tag{46}$$

The eight ellipse centers z_{cent} and rotations α are given in Table 1. The effective elastic moduli of (32) are computed by placing an increasing number of equi-sized quadrature panels on each ellipse. Estimated converged values for the effective moduli are presented in Table 2.

Figure 5 shows a convergence study of the Euclidean norm of the vector of elastic moduli $(c_{*1}, c_{*2}, c_{*3}, c_{*4}, c_{*5}, c_{*6})$ as the discretization is uniformly refined. The values in Table 2 are used as reference values when computing this norm. Note, in Figure 5, how stable the algorithm is. The estimated relative error converges to about $2 \cdot 10^{-13}$. The closest gap between two ellipse boundaries in the unit cell is approximately 0.001. This means that quantities related to the narrow neck between these two ellipses can be resolved with a relative accuracy of 0.001. On geometrical grounds we therefore estimate that the condition number of the problem is at most 10^3. As a consequence, we expect that it is possible, with an ideal algorithm, to compute effective elastic moduli with a relative accuracy not worse than $10^3 \cdot \epsilon_{\text{mach}} \approx 1 \cdot 10^{-13}$ in IEEE DP arithmetic. Our algorithm is close to this ideal.

The fine details of the curve in Figure 5 are, of course, dependent on how we choose the reference values of Table 2. Even though we get rather stable values for effective moduli

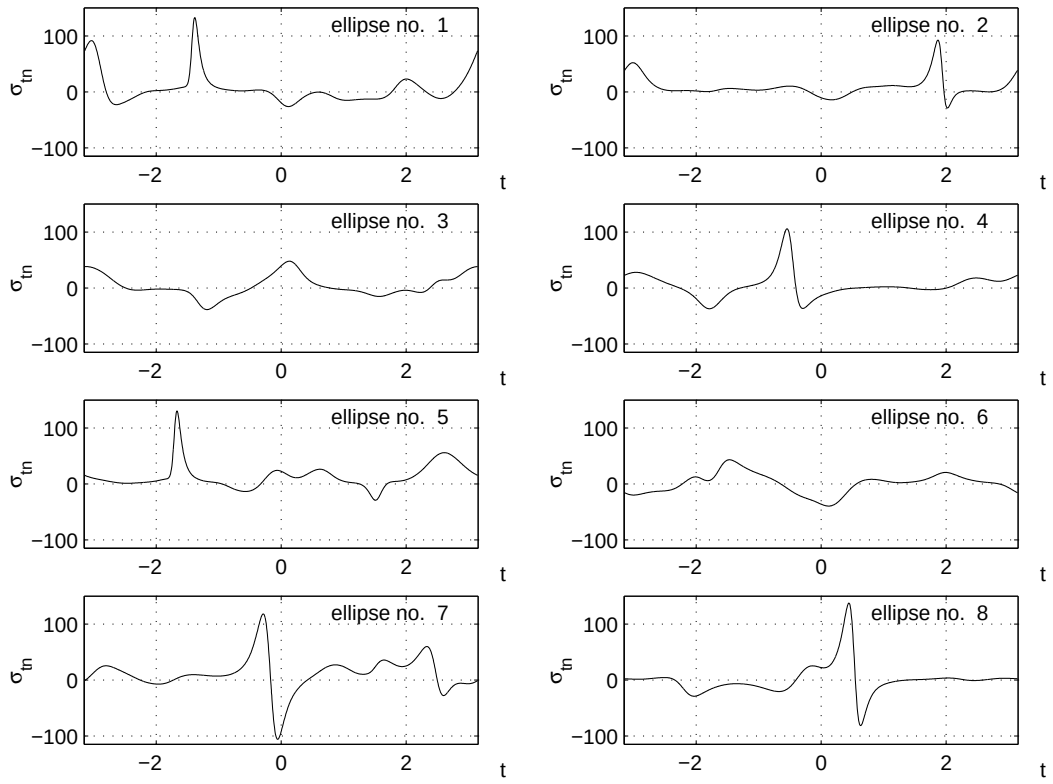

Figure 6: Normalized tangential stress $\sigma_{\rm tn}$ on the boundary of the eight ellipses of the geometry in Figure 4 under applied average stress $\bar{\sigma}_{\rm I} = (1, 0, 0)$.

already at 10,000 discretization points, corresponding to 80 panels on each ellipse, we believe that the values for around 100,000 discretization points are the most reliable. The reason for this is that our scheme for the evaluation of layer potentials close to their sources may introduce some inaccuracy in the last digits. At above 100,000 discretization points the interfaces are so overresolved that this scheme is not activated. In Figure 5, the stars refer to calculations done with the scheme activated, and open circles refer to calculations without this scheme. The GMRES iterations are terminated when the norm of the residual is smaller than $2 \cdot 10^{-15}$. This takes between 280 and 283 iterations for each of the applied average strains $\bar{\epsilon}_{\rm I}$, $\bar{\epsilon}_{\rm II}$, and $\bar{\epsilon}_{\rm III}$. The number of iterations needed is virtually independent of the number of discretization points used.

We also compute the normalized tangential stress $\sigma_{\rm tn}$ of (39). Figure 6 shows the normalized tangential stress on the boundaries of the eight ellipses for applied average stress $\bar{\sigma}_{\rm I}$.

12 Conclusions and outlook

The main advantage of equation (25) over the classic Sherman-Lauricella equation (14) is that we have omitted the need for the placement of the arbitrary points z_j. This, in turn, can substantially reduce the number of iterations needed to reach a given residual in

an iterative numerical algorithm. Other advantages include the reduction of the number of arbitrary constants, unification of formulations, simplified post-processing, and a more stable convergence.

Further, we conclude that the performance of our numerical algorithm based on equation (25) is very good. We establish agreement with previous authors (Haddon 1967; Ting, Chen, and Yang 1999) and greatly improve on the accuracy of their numerical results. Also, we demonstrate the stability of our algorithm on a setup involving eight closely spaced elliptical holes in a unit cell. The problem is resolved with a relative error smaller than 10^{-12} and the algorithm exhibits stability under extreme overresolution, extending up to half a million discretization points.

Still, for a plate with a single hole and with an underresolved calculation, the classic Sherman Lauricella (14) with an optimal placement of the arbitrary point z_j may give initially faster convergence than equation (25). The reason for this we ascribe to that, in our implementation, the part of the operator M_1 that describes self-interaction is implemented with 15th order accurate quadrature, while the operators M_2 and M_{SL} and the part of M_1 that describe interaction between different holes are 31st order accurate. We therefore speculate that it might be possible to find an even more efficient formulation, that always simultaneously improve on both (25) and (14).

13 Notation

α, β = forcing terms
D_1 = the interior of the perforated plane
D_2 = the interior of all holes
$\bar{\epsilon}_{ij}$ = averaged components of strain, $i, j = x$ or y
$\bar{\epsilon}$ = vector of averaged strain, $\bar{\epsilon} = (\bar{\epsilon}_{xx}, \bar{\epsilon}_{yy}, \bar{\epsilon}_{xy})$
$\bar{\epsilon}_{\mathrm{I}}, \bar{\epsilon}_{\mathrm{II}}, \bar{\epsilon}_{\mathrm{III}}$ = three fundamental vectors of prescribed average strain
ϕ, χ, ψ = elastic potentials, $\psi = \chi'$
Γ^j = the boundary of hole j
Γ = the union of all boundaries
K_t = stress concentration factor
κ = two-dimensional elastic bulk modulus
$M_1, M_2, M_{\mathrm{SL}}$ = integral operators
μ = two-dimensional elastic shear modulus
N = number of holes in the plane
(n_x, n_y) = normal unit vector on Γ
$\omega, \omega_{\mathrm{SL}}, \rho$ = unknown layer denities
σ_{ij} = components of stress, $i, j = x$ or y
$\bar{\sigma}_{ij}$ = averaged components of stress, $i, j = x$ or y
$\bar{\sigma}$ = vector of averaged stress, $\bar{\sigma} = (\bar{\sigma}_{xx}, \bar{\sigma}_{yy}, \bar{\sigma}_{xy})$
$\bar{\sigma}_{\mathrm{I}}, \bar{\sigma}_{\mathrm{II}}, \bar{\sigma}_{\mathrm{III}}$ = three fundamental vectors of prescribed average stress
σ_{tn} = normalized tangential stress
(t_x, t_y) = traction vector along a curve
u_i = displacement components, $i = x, y$

Remark 13.1 The two-dimensional bulk modulus κ is not identical to the three-dimensional

bulk modulus. For plane strain conditions, we have

$$\kappa = \frac{\mu}{1-2\nu}\,,$$

where ν is Poison's ratio. For plane stress conditions, we have

$$\kappa = \mu\frac{1+\nu}{1-\nu}\,.$$

Acknowledgement

This work was supported by NFR, TFR, and The Knut and Alice Wallenberg Foundation under TFR contracts 98-568 and 99-380.

References

Becker, A.A., 1992. The Boundary Element Method in Engineering, McGraw-Hill, London.

Carrier, J., Greengard, L., Rokhlin, V., 1988. A fast adaptive multipole algorithm for particle simulations, SIAM Journal on Scientific and Statistical Computing **9**, 669-686.

Dvorak, G.J., Srinivas, M.V., 1998. New estimates of overall properties of heterogeneous solids, Journal of the Mechanics and Physics of Solids **47**, 899-920.

Greengard, L., Helsing, J., 1998. On the Numerical Evaluation of Elastostatic Fields in Locally Isotropic Two-Dimensional Composites, Journal of the Mechanics and Physics of Solids **46**, 1441-1462.

Greengard, L., Kropinski, M.C., Mayo, A., 1996. Integral equation methods for Stokes flow and isotropic elasticity in the plane, Journal of Computational Physics **125**, 403-414.

Greengard, L., Rokhlin, V., 1987. A fast algorithm for particle simulations, Journal of Computational Physics **73**, 325-348.

Haddon, R.A., 1967. Stresses in an infinite plate with two unequal circular holes, Quarterly Journal of Mechanics and Applied Mathematics **20**, 277-291.

Helsing, J., 1996. Thin bridges in isotropic electrostatics, Journal of Computational Physics **127**, 142-151.

Helsing, J., Peters G., 1999. Integral equation methods and numerical solutions of crack and inclusion problems in planar elastostatics, SIAM Journal on Applied Mathematics **59**, 965-982.

Higham, N.J., 1996. Accuracy and stability of numerical algorithms, SAIM, Philadelphia, pp. 92-97.

Kahan, W., 1965. Further remarks on reducing truncation errors, Communications of the Association for Computing Machinery **8**, 40.

Lauricella, G., 1909. Sur l'intégration de l'équation relative à l'équilibre des plaques élastiques encastrées. Acta Mathematica **32**, 201-256.

Månsson, T., Nilsson, F., 2000. Nodule influence on fatigue crack growth thresholds in nodular cast iron, International Journal of Cast Metal Research **12**, 319-325.

Mikhlin, S.G., 1957. Integral equations, Pergamon Press, London.

Muskhelishvili, N.I., 1953. Some Basic Problems of the Mathematical Theory of Elasticity, P. Noordhoff Ltd, Groningen.

Neuber, H., 1937. Kerbspannungslehre, Springer Verlag, Berlin.

Parton, V.Z., Perlin, P.I., 1982. Integral Equation Methods in Elasticity, MIR, Moscow.

Persson, L.E., Persson, L., Svanstedt, N. Wyller, J., 1993. The homogenization method: an introduction, Studentlitteratur, Lund.

Radaj, D. and Schilberth G., 1977. Kerbspannungen an Ausschnitten und Einschlüssen, Deutscher Verlag für Schweisstechnik, Düsseldorf.

Rokhlin, V., 1985. Rapid solution of integral equations of classical potential theory, Journal of Computational Physics **60**, 187-207.

Saad, Y., Schultz, M.H., 1986. GMRES: a generalized minimum residual algorithm for solving nonsymmetric linear systems, SIAM Journal on Scientific and Statistical Computing **7**, 856-869.

Savin, G.N., 1961. Stress Concentration Around Holes, Pergamon Press, London.

Sherman, D.I., 1940. Sur la solution du second problème fondamental de la théorie statique plane de l'élasticité, Comptes Rendus (Doklady) de l'Académie des Sciences de l'URSS **28**, 25-32.

Sherman, D.I., 1959. On the problem of plane strain in non-homogeneous media, in Non-homogeneity in Elasticity and Plasticity, W. Olszak, ed., Pergamon Press, 3-20.

Sokholnikoff, I.S., 1956. Mathematical Theory of Elasticity, McGraw-Hill, New York.

Ting, K., Chen, K.T., Yang, W.S., 1999. Applied alternating method to analyze the stress concentration around interacting multiple circular holes in an infinite domain, International Journal of Solids and Structures **36**, 533-556.

Vigdergauz, S., 2000. Complete Elasticity Solution to the Stress Problem in a Planar Grained Structure, Mathematics and Mechanics of Solids **4**, 407-439.